Use of Polarization to Characterize Precipitation and Discriminate Large Hail

N. BALAKRISHNAN AND D. S. ZRNIĆ

NOAA/Environmental Research Laboratories, National Severe Storms Laboratory, Norman, Oklahoma

(Manuscript received 30 June 1989, in final form 9 November 1989)

ABSTRACT

We examine the utility of the correlation coefficient between linear orthogonally polarized echoes for determining precipitation type and gauging hail size. Models and measurements from pure rain coincide in predicting very high correlations (0.98); similar results are obtained with pure hail. Several mechanisms could cause the lowering of correlation but the behavior of the examined data is definitely attributed to a mixture of hydrometeor types. This decrease is an indicator of hail size; it is shown theoretically that in at least two other realistic situations the correlation would decrease with hail size. For the examined case a model of hail shape and orientation during fall is able to reproduce the essential features of polarimetric measurements. It suggests, together with our data and data from other investigators, that substantial negative differential reflectivity (about −1 dB) in a region of high reflectivity factor values is caused by hailstones larger than about 2 cm in diameter.

1. Introduction

Polarimetric radar measurements provide bulk estimates of the shapes of the ensemble of hydrometeors in the radar resolution volume. There is evidence supported by theory (Green 1975) and wind tunnel observations (Pruppacher and Pitter 1971) that the shape of a rain drop is related to its size. Also, rain drops exhibit little or no canting and fall with their minor axes oriented vertically (Meischner et al. 1989; Antar and Hendry 1985). It was first shown by Seliga and Bringi (1976) that the existence of such accurate relation between rain drop shape and size can be exploited to obtain an improved estimation of rainfall from polarimetric measurements. They demonstrated that the differential reflectivity Z_{DR} in rain medium is related to the median volume diameter D_0. The Z_{DR} and D_0 are measures of the mean of the reflectivity-weighted axis ratio and volume-weighted size distribution of rain drops, respectively (Jameson 1983, 1987).

The differential propagation constant K_{DP} (here defined as twice the difference between propagation constants for horizontally and vertically polarized waves) is another parameter that coherent polarimetric radars can measure. It is dependent on the forward propagation characteristics, but can be obtained through an appropriate processing of the backscattered echoes (Mueller 1984; Jameson and Mueller 1985; Sachidananda and Zrnić 1986). The K_{DP} is a measure of the mean of the mass-weighted axis ratio of the drops (Jameson 1985). Sachidananda and Zrnić (1987) established an empirical relation between K_{DP} and rain rate R. Thus, the basis of polarimetric rain rate estimation is that the average measure of shape given by Z_{DR} is related to the average measure of size D_0 and that K_{DP} is almost linearly related to the rain rate R. In essence, Z_{DR} and K_{DP} are parameters that give additional information about the drop size distribution, and hence make possible an improved estimation of rain rate.

The effectiveness of shape dependence on diameter that allows quantification of rainfall is reduced by several factors when other types of hydrometeors are encountered. For a given shape (axis ratio) and size distribution of hydrometeors, the Z_{DR} and K_{DP} depend on the extent to which the relative dielectric constant of the hydrometeors differ from unity. Because liquid water has a relative dielectric constant of about 80, whereas ice has a value of about 3, it is evident that Z_{DR} and K_{DP} would be more effective with water particles than with ice forms (Battan 1966, p. 38). Also, for ice precipitation, there are no unique relationships between particle size and shape. For example, hailstones are sometimes well represented by spheroids whose oblateness nearly increases with diameter (Knight 1986) and may exhibit tumbling motion when they fall (Pruppacher and Klett 1978; Knight and Knight 1970). The tumbling motion reduces the capability to deduce the shape of the hydrometeors. It changes the relation between the observed radar parameters and size of the hydrometeors that seem to the radar to be more spherical. When the tumbling is completely random, Z_{DR} and K_{DP} become zero. Thus, whenever precipitation includes ice forms, the quantitative interpretation of Z_{DR} and K_{DP} becomes more

Corresponding author address: Dr. Dusan S. Zrnić, NOAA/ERL, National Severe Storms Laboratory, 1313 Halley Circle, Norman, OK 73069.

difficult. In such situations, Z_{DR} and K_{DP} have been used mainly to infer the presence of ice forms, but not to estimate their fall rates. For example Leitao and Watson (1984) as well as Aydin et al. (1986) developed a technique to identify hail from Z_H and Z_{DR} whereas Zrnić et al. (1988) proposed Z_H and K_{DP} measurements for that purpose.

It is shown here that the ambiguity in the interpretation of Z_{DR} and K_{DP}, particularly in precipitation that includes hail and other ice forms, can be reduced to an extent by the measurement of the correlation $\rho_{HV}(0)$, at zero time lag, between horizontally and vertically polarized radar echoes. We first examine the physical factors that contribute to the decorrelation between orthogonally polarized echoes. We resort to model simulation to bring out the potential use of $\rho_{HV}(0)$ for probing precipitation that consists of rain, rain–hail mixtures, or hail. All our calculations are for a wavelength of 10 cm, which is also the wavelength of the forthcoming Next Generation Weather Radar (NEXRAD). In an attempt to categorize hail size we investigate the effects that various hailstone models have on the differential reflectivity and the correlation coefficient. An estimator for $\rho_{HV}(0)$ in radars that use alternating sequences of horizontal and vertical polarizations is given in Appendix A. From analysis of statistical error in radar estimation of $\rho_{HV}(0)$ and simulation, it is suggested that $\rho_{HV}(0)$ can be useful to identify hydrometeors and to gauge hail size qualitatively. But our data as well as data from other investigators and model calculations suggest that negative Z_{DR} near -1 dB indicate presence of large hail (>2 cm in diameter). Radar measurements of $\rho_{HV}(0)$ and other polarimetric variables from a few Oklahoma storms are shown to substantiate these predictions.

2. Correlation $\rho_{HV}(0)$ between horizontally and vertically polarized echoes

For a distribution of hydrometeors, the correlation $\rho_{HV}(0)$ between horizontally and vertically polarized echoes is defined as

$$\rho_{HV}(0) = \frac{|\langle S_H^i S_V^{i*}\rangle|}{[\langle|S_H^i|^2\rangle\langle|S_V^i|^2\rangle]^{0.5}}, \qquad (1)$$

where S_H^i and S_V^i are scattering coefficients of the ith hydrometeor at horizontal and vertical polarizations and the angle brackets represent average over the ensemble. In general, these coefficients contain phase factors, and their difference $\delta = (\delta_H^i - \delta_V^i)$ is the differential phase shift due to scattering. The ensemble average in Eq. (1) is over the size (diameter) and shape (axis ratio) distribution of the hydrometeors. Similar definition of $\rho_{HV}(0)$ by Sachidananda and Zrnić (1985) as well as by Jameson (1987) ignores the effects of differential phase shift due to scattering because these authors consider situations where such effects are small (i.e., Rayleigh scattering). We retain the term because it is significant even at 10 cm wavelength for hailstones.

It is convenient to rewrite Eq. (1) as

$$\rho_{HV}(0) = \frac{|\langle (Z_{DR}^i)^{0.5}\,|S_V^i|^2 \exp[j(\delta_H^i - \delta_V^i)]\rangle|}{\bar{Z}_{DR}^{0.5}\bar{S}_V^{\,2}}, \qquad (2)$$

where Z_{DR}^i is the differential reflectivity of the ith hydrometeor and the mean Z_{DR} is expressed as a ratio

$$Z_{DR} = \frac{\langle|S_H^i|^2\rangle}{\langle|S_V^i|^2\rangle}. \qquad (3)$$

Here we use either this ratio form or decibel unit for Z_{DR}, and state which one it is whenever needed.

3. Effects that influence the correlation

There are several meteorological factors that influence $\rho_{HV}(0)$. From Eq. (2) we see that these are related to apparent shape (through Z_{DR}), size, and differential shift upon scattering. In nature these factors most often occur simultaneously. For rain the distribution of sizes (characterized with equivalent volume diameters) and the distribution of shapes (characterized with axis ratios) are closely related. Nevertheless, we discuss each cause under a separate heading to simplify the analysis and account whenever possible for each effect individually. The effects that we consider are shape distribution, size distribution, distribution of differential phase shift upon scattering, irregular shape of hydrometeors, and mixtures of two types of hydrometeors. The differential phase shift upon scattering is significant for Mie scatterers only. All the other listed effects are significant for both Mie and Rayleigh scatterers.

a. Shape distribution of hydrometeors

Oblate spheroids closely approximate the shape of rain drops. The oblateness of a rain drop increases with its size. The ratio of minor to major axis a/b, is related to the equivalent volume drop diameter D (in mm) by (Pruppacher and Pitter 1971)

$$a/b = 1.03 - 0.062D \qquad (4)$$

At 10 cm wavelength, rain drops are small enough to be approximated as Rayleigh scatterers. Because of increasing oblateness, Z_{DR} of rain drops increases with size. For an ensemble of rain drops, it is affected mainly by the mean shape (axis ratio) and is weakly dependent on the distribution of shapes within the ensemble (Jameson 1983). In contrast, it can be deduced from Eq. (2) that $\rho_{HV}(0)$ is influenced by the distribution of the shapes within the ensemble (Jameson 1987; Jameson and Dave 1988). The physical reason for this dependence is that changes in reflectivities at horizontal and vertical polarization are not equal for the same increment in sizes. To give the reader an idea about the subtle difference in the dependence of Z_{DR} and

$\rho_{HV}(0)$ on the distribution of shapes we use the following artificial examples.

The Z_{DR} of a monodispersed rain consisting of 4-mm rain drops is 2.5 dB, and its $\rho_{HV}(0)$ is unity. Z_{DR} is unaffected when the shape distribution is broadened by combining 2-, 4-, and 6-mm-diameter rain drops, with axis ratio given by Eq. (4) and a number concentration ratio of 200:1:0.01. However, $\rho_{HV}(0)$ of such a distribution is reduced to 0.988.

To further illustrate the effects of the distribution of shapes consider infinitesimally thin cylinders each of which is either horizontal or vertical and contrast this to spherical particles. These are extreme examples of differences between the horizontal and vertical dimensions of individual particles. It can be deduced from Eq. (2) that $\rho_{HV}(0)$ is zero for the cylinders. For the special case when half of the cylinders are oriented horizontally and the other half vertically, Z_{DR} is 0 dB. Distribution of spherical hydrometeors has the same Z_{DR}, but its $\rho_{HV}(0)$ is 1.

Thus, $\rho_{HV}(0)$ of a distribution of hydrometeors is lowered whenever both exaggerated oblate and exaggerated prolate shapes (compared to the mean shape) are present. Calculations for a range of rain rates up to 200 mm h^{-1} (Sachidananda and Zrnić 1985) indicate that the effects of shape on the correlation coefficient from rain are small; the values are larger than 0.99. Jameson (1987) and Jameson and Dave (1988) considered mainly the shape effects on $\rho_{HV}(0)$, and observed that $\rho_{HV}(0)$ is dependent on the breadth of the axis ratio distribution.

It is useful to examine the behavior of $\rho_{HV}(0)$ for a typical drop size distribution (DSD) because, as we shall see shortly, it may provide means to discriminate between pure rain and mixed-phase precipitation. Consider a gamma DSD of the form

$$N(D) = N_0 D^{\mu} \exp(-\Lambda D), \qquad (5)$$

where N_0, Λ, and μ are the intercept, slope, and shape parameters of the distribution.

Both Z_{DR} and $\rho_{HV}(0)$ are independent of N_0. The variations of Z_{DR} and $\rho_{HV}(0)$ are shown in Fig. 1a with μ as a parameter. To generate this figure, complex scattering coefficients were obtained by the extended T-matrix method (Barber and Yeh 1975), and the drop shape given by Eq. (4) was used. Note that the theoretical curve is slightly lower than the curve presented by Sachidananda and Zrnić (1985). We attribute this to the differential phase shift upon scattering that is included in the present computations. The scattergram of $\rho_{HV}(0)$, Z_{DR} in Fig. 1b was obtained from a rainstorm in Oklahoma, as was the scattergram of $\rho_{HV}(0)$, Z in Fig. 2a. The reflectivity factor Z (dBZ) is an average (obtained in real time) of the reflectivity factors Z_H (dBZ) and Z_V (dBZ). The data in Fig. 1b and Fig. 2a were collected with a 10-cm-wavelength radar performing sector scans at a fixed elevation of 1°. We have confidence in the data with reflectivity factor values larger than 35 dBZ because these correspond to strong signal to noise ratios and have little contamination from sidelobes; only such data will be used for interpretations. Overall the measurements fall within the range of the theoretical curves and have a similar tendency as seen from decreasing $\rho_{HV}(0)$ with increasing Z_{DR} and Z_H, although they have a negative offset of about 0.01 (Fig. 2b). This offset is not surprising considering that the theory does not include several effects (e.g., canting and oscillation of drops, non-Gaussian spectral shapes, noise, and even statistical uncertainty that produces a small negative bias). The form of the estimator (Appendix A) is such that it produces a bias for values of the correlation coefficient near 1. More than 20,000 points are contained in the scattergrams, and as seen in Fig. 2b the mean of the correlation coefficient for reflectivities larger than 30 dBZ is 0.98. At smaller reflectivities the signal-to-noise ratio is lower, and the additive white noise causes the decrease seen in Fig. 2b. Almost identical results were obtained from another rain case in Oklahoma (Balakrishnan and Zrnić 1989), which leads us to believe that the mean correlation coefficient from pure rain

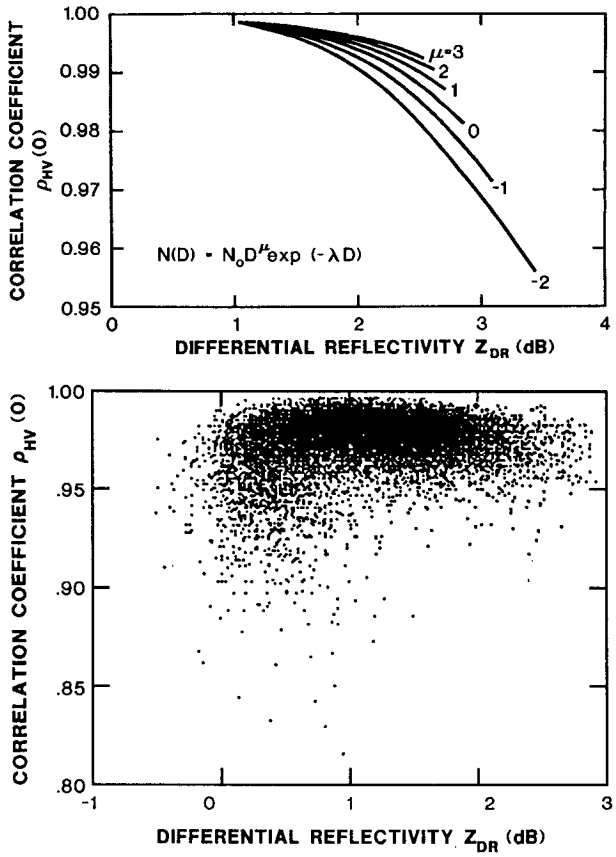

FIG. 1. (a) Theoretical relationship between $\rho_{HV}(0)$ and Z_{DR} for a gamma drop size distribution. The exponent μ is variable. (b) Scattergram $\rho_{HV}(0)$, Z_{DR} obtained from a rain storm on 6 June 1986, in Oklahoma at a range between 38 and 68 km.)

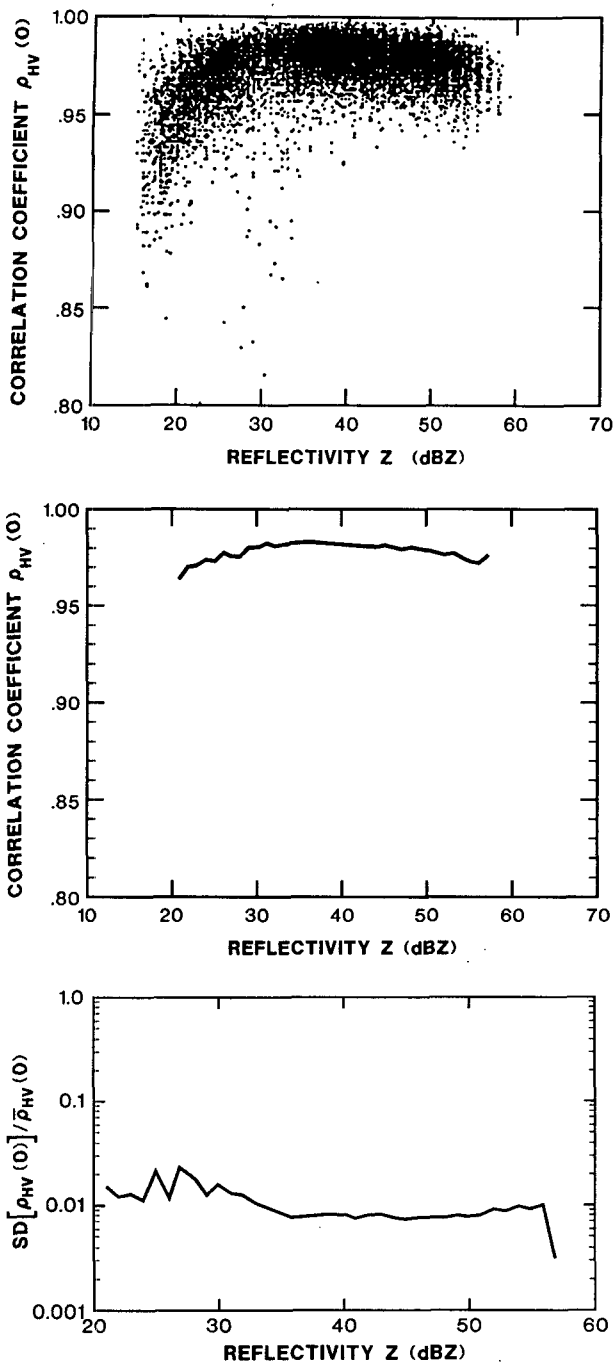

FIG. 2. (a) Scattergram $\rho_{HV}(0)$, $Z = (Z_H + Z_V)/2$ from the same rain storm as in Fig. 1b. (b) Mean values of the correlation coefficient for the scattergram in (a). (c) Standard error of the mean estimates in (b).

would be larger than about 0.97. The standard error about the mean in Fig. 2b is shown in Fig. 2c to be near 0.01.

It was shown by Jameson and Dave (1988) that it may be theoretically possible to use $\rho_{HV}(0)$ to explain the discrepancy between surface-measured rain rate and that estimated from radar-measured Z_H and Z_{DR} (Goddard and Cherry 1984). An alternative approach for the use of $\rho_{HV}(0)$ in polarimetric rain rate estimation is suggested next.

Rain rate estimation from the measurement of Z_H and Z_{DR} hinges on the assumptions (Seliga and Bringi 1976) that (i) the relationship of axis ratio to diameter is known a priori, (ii) the rain drops are oriented with their minor axes vertical, and (iii) the drop size distribution is of the exponential type with two unknown parameters and large D_{max}. Deviation from any or all of these assumptions may occur in nature. This causes a bias in the measurement of Z_{DR} and rain rate. From radar measurement it is not possible to identify or to account for the deviations from each of the listed assumptions. A reasonable approach is then to treat all the bias in Z_{DR} as if it were caused by an equivalent change in assumed drop shape (Goddard and Cherry 1984) or in the drop size distribution (Ulbrich and Atlas 1984). In either case, a third remote measurable (Ulbrich and Atlas 1984) can in principle identify and estimate the bias in Z_{DR}. The $\rho_{HV}(0)$ could be a third measurable. From measured Z_{DR} and $\rho_{HV}(0)$ it is possible to obtain μ from Fig. 1a. Once μ is known, Λ and N_0 can be obtained from Z_H and Z_{DR} (Seliga and Bringi 1978).

Though, in principle, it is possible to obtain improved rain rate estimates using $\rho_{HV}(0)$, the practical utility for such an application using linear polarizations may be limited. For example, 128 sample pairs (i.e., 256 pulses) are needed to estimate $\rho_{HV}(0)$ with a standard error of about 0.1 if the spectrum width is 4 m s^{-1} (see Appendix A). Averaging nine samples in range spaced 150 m apart would reduce the error to 0.03; this may be acceptable for estimating μ at higher rain rates if a long dwell time can be tolerated. But the rain rate estimated by inclusion of more parameters is inferior to the estimate from the differential propagation constant. This parameter is available from coherent polarimetric radars. The potential to use $\rho_{HV}(0)$ in rainfall estimation with circularly polarized radars should be explored because measurements are simultaneous with no switching problems and therefore the errors are expected to be smaller.

b. *Size distribution*

Because the shape of hailstones is not known precisely, and to simplify calculations and bring the number a variable to a manageable few, in this paper we approximate hailstones with oblate spheroids. Ground observations (Knight 1986; Matson and Huggins 1980) indicate that the majority of hailstones have axis ratios close to 0.8, and diameters large enough to be treated in the Mie scattering regime at 10 cm wavelength. Even when the actual shape of the hailstones does not vary with size, the apparent shape, as indicated by Z_{DR} of these Mie scatterers, does. The differential reflectivity

of dry (oblate, minor axis vertical) hailstones decreases gradually and changes sign at a diameter of 5 cm (Seliga and Bringi 1978). Wet and spongy spheroids exhibit much larger and more rapid variability of Z_{DR} with size (Longtin et al. 1987). Horizontally and vertically polarized echoes from hailstones with substantial variability of Z_{DR} would be less correlated with each other than echoes from hailstones that have slowly changing Z_{DR} with size. This is because ρ_{HV} is smoothed by the distribution function of sizes. Thus, we conclude that if large hail were approximately oblate, oriented, and dry there would be little or no decrease of ρ_{HV} compared with small hail. But wet (or spongy) oblate hail would cause a significant decrease in ρ_{HV} when size reaches about 5 cm. It just might be possible to categorize hail size from measurements of ρ_{HV} below the melting level if it were preferentially oriented. Hail orientation is discussed further in section 3d.

c. *Distribution of the differential phase shift upon scattering*

Use of differential phase shift upon scattering, δ, to distinguish Rayleigh scatterers such as rain drops from non-Rayleigh scatterers such as hailstones, was first proposed by McCormick and Hendry (1975). The radar measurables like Z_H and Z_{DR} are not dependent on δ, but $\rho_{HV}(0)$ is affected by the distribution of δ around its mean and K_{DP} depends on the mean canting angle.

The variations of δ with diameter for wet, dry, and spongy hail are plotted in Fig. 3. They were calculated using the extended T-matrix method (Barber and Yeh 1975). The axis ratio is assumed to be 0.8 for wet and dry hail, and the minor axis is oriented vertically in the plane of polarization. This particular model deliberately ignores canting and azimuthal orientation of spheroids. Its sole purpose is to provide qualitative order of magnitude information about values to be expected in measurements. It can be argued that inclusion of canting angle variations and random azimuthal orientation would be equivalent to the simple model but with an effective larger axial ratio. A more complicated model that allows random azimuthal orientation and in which the minor axis is canted 90° is treated later. The dielectric constant of wet hail is taken as that of liquid water ($9.0585 + 1.3421j$) at 10-cm wavelength (Warner 1978), and the dielectric constant of spongy hail with 40% water is obtained from the mixture formula given in Longtin et al. (1987). This particular percentage was chosen because it produces scattering coefficients that appear to differ most from those of wet and dry hail. Thus the three models (dry, wet and spongy hail) can be used to deduce qualitatively the properties of hail.

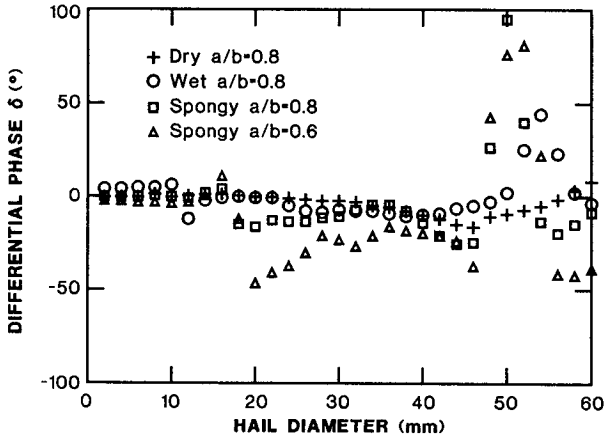

FIG. 3. Differential phase shift upon scattering vs diameter for oblate hail. The minor to major axis ratio is a/b, the minor axis is vertical in the plane of polarization, and the phase state of hail is indicated. Spongy hail consists of 40% liquid water.

It is seen from Fig. 3 that δ varies between $-50°$ and $+90°$ for spongy hail and between $-10°$ and $45°$ for wet hail. Although the relative dielectric constant of wet hail is larger than of spongy hail, resonance in the Mie scattering regime causes δ to be larger (at the same axis ratio) for spongy hail. The effective width of the distribution of δ, and hence the reduction in $\rho_{HV}(0)$, is influenced by the hail size distribution. We see from Fig. 3 that for size distributions containing larger hail the distribution of δ will be wider, and hence $\rho_{HV}(0)$ will be smaller. It is again apparent that wet and spongy hailstones produce substantial variations of δ starting at about 5 cm. This is also where Z_{DR} changes. Therefore if hailstones of this size and shape were present in sufficient number they would produce a large decrease in ρ_{HV}. However, δ of dry hail (dielectric constant of ice, $1.78 + 0.007j$) and rain drops [axis ratio as in Eq. (4)] is small. For dry hail with a 0.8 axis ratio and 60-mm diameter δ is 8.25° (Warner 1978) and for a 6 mm rain drop δ is about 0.2°. Hence, the effect of δ on $\rho_{HV}(0)$ in rain and dry hail may not be significant.

The decorrelation effect of δ is similar to that caused by the Doppler spectrum width (Doviak and Zrnić 1984) except that it is independent of the pulse spacing. In a weather radar with an unambiguous velocity of 34 m s^{-1}, a spectrum width of 2 m s^{-1} (10.6° rms phase shift) produces decorrelation between successive radar echoes of 0.983 (Doviak and Zrnić 1984). With the spectrum width of 4 m s^{-1}, which is a median in severe storms, the correlation drops to 0.934.

d. *Distribution of orientations*

1) CANTING ANGLE DISTRIBUTION

The change in $\rho_{HV}(0)$ due to the distribution of canting angles is dependent on mean orientation, shape, and size of the hydrometeors. In a monodisperse (shape and size) ensemble of aligned spheroids [$\rho_{HV}(0) = 1$], $\rho_{HV}(0)$ begins to decrease with increasing breadth of the canting angle distribution. Canting changes the effective shape of the hydrometeors as seen by the radar.

The distribution of canting angles inferred with circular polarization radars as an indicator of the degree of common alignment among hydrometeors in the radar resolution volume (Hendry et al. 1976). Observational evidences show that the degree of common alignment is much less in hail medium than in rain. Hence, the effect of canting is of significance mostly in hail storms.

Canting modifies the effective scattering matrix of hydrometeors. We write the scattering matrix of an uncanted (aligned with the reference direction) spheroidal hydrometeor as

$$S = \begin{bmatrix} S_H & 0 \\ 0 & S_V \end{bmatrix}, \tag{6}$$

where S_H and S_V are the complex scattering coefficients. From Stapor and Pratt (1984) and Holt (1984), it can be shown that the scattering matrix modified by canting is

$$\mathbf{S}' = \mathbf{T}_1 + \mathbf{T}_2 + \mathbf{T}_3,$$

where

$$\mathbf{T}_1 = \frac{1}{2}\begin{bmatrix} (S_H - S_V)\cos 2\alpha & 0 \\ 0 & -(S_H - S_V)\cos 2\alpha \end{bmatrix},$$

$$\mathbf{T}_2 = \frac{1}{2}\begin{bmatrix} (S_H + S_V) & 0 \\ 0 & (S_H + S_V) \end{bmatrix},$$

and

$$\mathbf{T}_3 = \frac{1}{2}\begin{bmatrix} 0 & (S_H - S_V)\sin 2\alpha \\ (S_H - S_V)\sin 2\alpha & 0 \end{bmatrix};$$

α is the canting angle (measured from vertical) in the plane of polarization, $\mathbf{T}_2$ is independent of canting, and $\mathbf{T}_3$ is not relevant in radars (such as the NSSL radar) that do not process the cross-polarized echoes. Extending Eq. (6) to hydrometeor canting in planes other than the plane of polarization is straightforward (Holt 1984).

There are no known physical relationships between canting angles and hydrometeor size or shape. Hence, the canting angle distribution in most earlier work (Holt 1984; McCormick and Hendry 1975; Metcalf 1988) was assumed to be independent of the hydrometeor size or shape distributions. Therefore we also adopt the assumption, and with this proviso $\rho_{HV}(0)$ for a distribution of hydrometeors can be written from Eqs. (1) and (6) as

$$\rho_{HV}(0) = \frac{-\langle R_1R_1^*\rangle\langle\cos^2 2\alpha\rangle + \langle R_2R_2^*\rangle - 2\,\mathrm{Im}\langle R_2R_1^*\rangle\langle\cos 2\alpha\rangle}{[\{\langle R_1R_1^*\rangle\langle\cos^2 2\alpha\rangle + \langle R_2R_2^*\rangle + 2\,\mathrm{Re}\langle R_2R_1^*\rangle\langle\cos 2\alpha\rangle\}\{\langle R_1R_1^*\rangle\langle\cos^2 2\alpha\rangle + \langle R_2R_2^*\rangle - 2\,\mathrm{Re}\langle R_2R_1^*\rangle\langle\cos 2\alpha\rangle\}]^{0.5}} \tag{7a}$$

where R_1 and R_2 are related to the circular polarization observables W, W_1 and W_2 (Holt 1984) by

$$\langle R_2R_2^*\rangle = W_2 = \langle (S_H + S_V)(S_H^* + S_V^*)\rangle$$

$$\langle R_1R_1^*\rangle = W_1 = \langle (S_H - S_V)(S_H^* - S_V^*)\rangle$$

$$\langle R_1R_2^*\rangle = W = \langle (S_H + S_V)(S_H^* - S_V^*)\rangle. \tag{7b}$$

The expectations involving scattering coefficients in Eq. (7) are taken over the size distribution, and those involving α are over an assumed canting angle distribution.

Next we show the connection between the circular depolarization ratio (CDR) and ρ_{HV} because the relationship of the former to some precipitation types has been investigated previously (Barge 1972; Hendry et al. 1976). That allows extension of known results to be made to the less studied ρ_{HV}. The circular depolarization ratio is defined as (Holt 1984)

$$\mathrm{CDR} = 10\log(W_1/W_2), \tag{8}$$

When the canting angle distribution is uniform over the interval $-\pi/2 < \alpha < \pi/2$, $\langle\cos 2\alpha\rangle$ is zero and $\langle\cos^2 2\alpha\rangle = 0.5$. Equation (7a) then reduces to

$$\rho_{HV}(0) = \frac{2 - 10^{0.1\,\mathrm{CDR}}}{2 + 10^{0.1\,\mathrm{CDR}}}. \tag{9}$$

This relation is similar in form to that involving the correlation coefficient between co- and cross-circular polarization echoes and Z_{DR} (McCormick 1979). This is not surprising because the echoes of circularly polarized waves from oriented scatterers would have properties similar to those of echoes of linearly polarized waves from randomly distributed scatterers (Born and Wolf 1951).

The variation of $\rho_{HV}(0)$ with CDR is plotted in Fig. 4. In Eq. (9) and in Fig. 4 CDR corresponds to noncanted hydrometeors whereas $\rho_{HV}(0)$ is for a uniform distribution of canting angles. Therefore the region between $\rho_{HV}(0) = 1$ and the curve represents a range of values that may be possible for oblate spheroids. The plot is instructive with the labeling (see abscissa in Fig. 4) that corresponds to CDR of known hydrometeors. From the measurements of Barge (1972) and Hendry et al. (1976) it can be seen that CDR is less than -15 dB in rain (it is lower in stratiform rain than in convective rain); CDR can be as high as -5 dB in hail and is larger in storms that produce larger size hail. Also, the degree of common alignment is much less in hail than in rain. Thus, the interpretation of Fig. 4 in light of the observation by Barge (1972) and Hendry et al. (1976) suggests that the presence of larger diameter hail could result in lower $\rho_{HV}(0)$.

McCormick and Hendry (1975) proposed a model

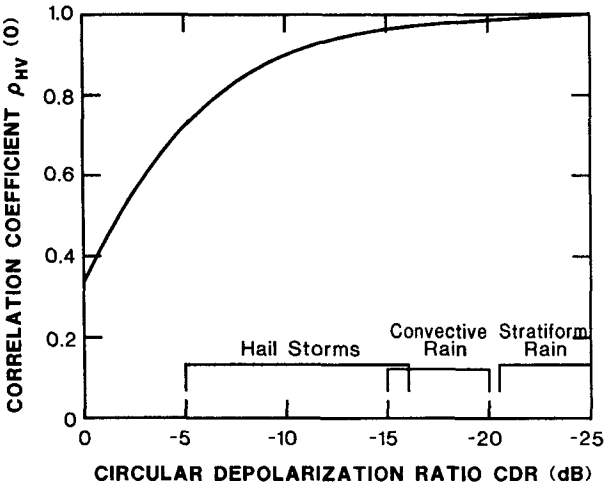

FIG. 4. Relationship between $\rho_{HV}(0)$ of randomly canted oblate spheroids with the minor axis in the plane of polarization. The CDR is for oriented spheroids.

for the distribution of canting angles that is related to the theory of partial polarization. In this model, the apparent distribution of canting angles is described by a fraction of scatterers that have a fixed orientation (say α_o), whereas the complementary fraction has a uniform distribution of canting angles. Although this model does not occur in nature it is instructive because it can illustrate the effects of random orientation. The $\rho_{HV}(0)$ for this model can be obtained from Eq. (7a); it is plotted in Fig. 5 for wet hailstones with $\alpha_o = 0°$. The axis ratio dependence on size is taken from measurements in Oklahoma tabulated by Knight (1986). Figure 5 shows that $\rho_{HV}(0)$ can be as low as 0.9 when hail size is greater than 5 cm, even when only 25% of the hailstones are randomly oriented. Increasing the percentage of randomly oriented scatterers in the plane of polarization for this monodisperse size distribution of hailstones decreases $\rho_{HV}(0)$. This aspect of $\rho_{HV}(0)$, the cross-correlation between horizontally and vertically polarized echoes, is in contrast to that of the amplitude of the correlation between left and right circularly polarized echoes (ORTT in the notation of McCormick and Hendry 1975). ORTT is zero whenever Z_{DR} is 0 dB and the orientation of the hydrometeors is random.

2) RANDOM ORIENTATION OF OBLATE SPHEROIDS

The models described in the previous section are not realistic in that they treat only canting of hydrometeors in the plane of polarization. Physical considerations by List (1985) suggest that rotation about the minor axis and slight precession about the horizontal is one possible stable mode for hail fall. This is consistent with observations that in oblate spheroidal hail the thickness of homogeneous layers is largest at the equator and smallest at the poles. Thus during the growth stage such hailstones must have spent most of their time in a position that offers favorable growth to the equatorial region. The fact that the thickness of layers at the equator is fairly uniform suggests that such hailstones rotate during growth and, if large enough, they probably continue to fall in this mode below the melting level. Furthermore, beyond the embryo stage the basic spheroidal symmetry is not changed by the growth (which is primarily from accretion of a unidirectional flux of droplets) implying an equal exposure of symmetrically equivalent surface points (any two circles about the minor axis and equidistant from the plane of major axes, Kry and List 1974). Although it is not known whether this model typifies hailstones there is one more reason to consider oblate spheroids having a symmetry (minor) axis in a horizontal plane. Namely such model can explain, in a qualitative sense, our observations as well as some observations of other investigators. Because there are no physical reasons to expect preferential alignment of the minor axes we assume that they are uniformly distributed in the horizontal plane ($\alpha = \pi/2$). For this model, the modified scattering coefficients S'_H and S'_V are given by

$$S'_H = S_H \cos^2(\phi) + S_V \sin^2(\phi)$$
$$S'_V = S_H \qquad (10)$$

where ϕ is the azimuthal angle measured in the horizontal plane with respect to the direction of propagation. Canting that would model gyration of the minor axis is not introduced in our model because it complicates calculations. Qualitative results for small canting angles can be obtained by using larger axis ratio (i.e., less oblate hailstones); because we consider a range of ratios from 0.6 to 0.9, the absence of canting does not change our conclusions.

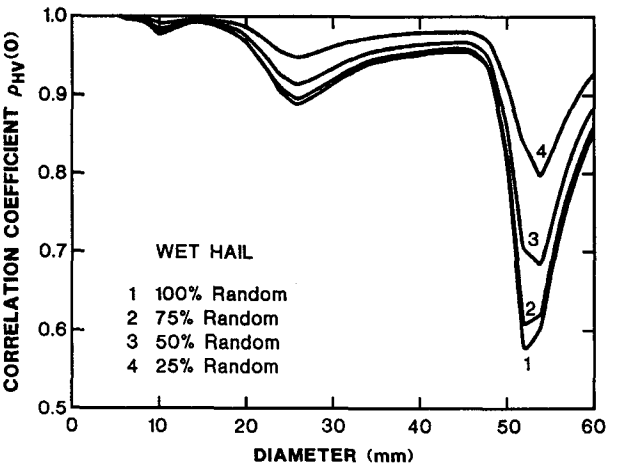

FIG. 5. Correlation coefficient as a function of diameter of oblate wet spheroids. The axis ratios are taken from Knight (1986), and the fraction of randomly oriented (in the plane of polarization) scatterers is indicated. The minor axis of the aligned scatterers is vertical.

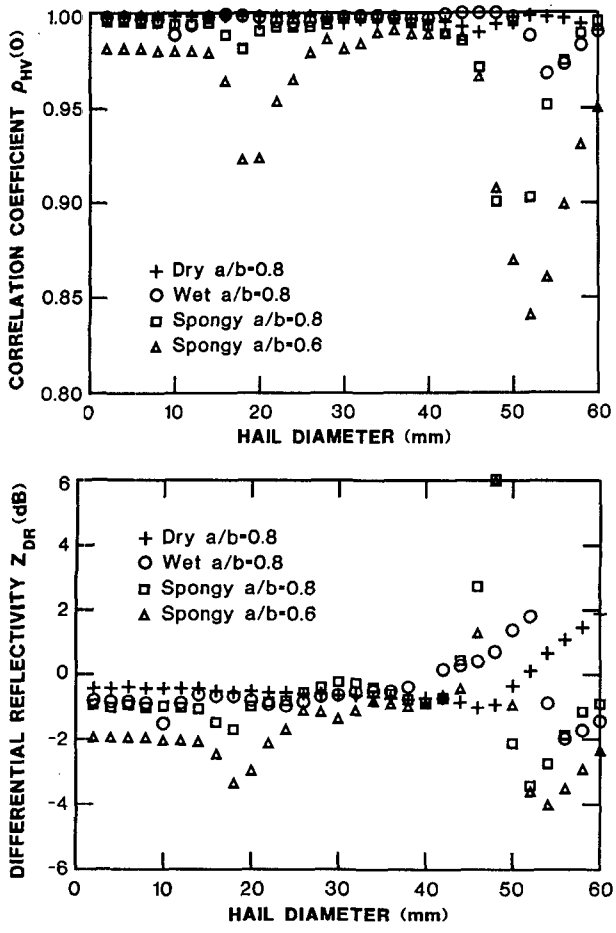

FIG. 6. (a) Correlation coefficient as a function of diameter for oblate spheroids. Modeled are wet, dry, and spongy hail; axis ratios are indicated. Hailstones have minor axis randomly oriented in the horizontal plane. (b) Differential reflectivity as a function of diameters for the same model as in (a).

Figure 6a reveals that wet (axis ratio of 0.8) as well as spongy hailstones (axis ratio of 0.6 and 0.8) about 5 cm in size might lower the correlation if they are present in sufficient numbers to contribute significantly to the radar echoes. But the effects of dry hail would not be measurable because the variation of ρ_{HV} up to 6 cm in size is only about 0.01.

Because this model fits some of our data we include in Fig. 6b the differential reflectivity that is used in Section 5 to check for consistency with the correlation coefficient. Differential reflectivity also exhibits significant change at a size of about 5 cm. Near 2 cm both ρ_{HV} and Z_{DR} (for spongy hail with axis ratio of 0.6) depart from their neighborhood values, and a slightly smaller deviation due to Mie scattering effects (not shown) occurs for wet hail with a 0.6 axis ratio. There are at least two reasons why this departure would be hard to detect in data. First, it occurs at low axis ratios (0.6) and size $\sim$ 2 cm. Experimental indications (Knight 1986) are that such low axis ratios are more common in hail larger than 2 cm. Second, because this is confined to a narrow region near 2 cm the effects would be smoothed by the hail size distribution.

e. *Irregular shape of hydrometeors*

Larger hailstones (4–10 cm diameter) are roughly irregular with small and large protuberances (List 1985). That is to say that hailstones do not obey fractal laws, so the protuberance-to-diameter ratio is not constant, but may increase with hailstone size. Although this is not always the case, when true it will result in a noticeable decrease of $\rho_{HV}(0)$. Occurrence of such irregular shapes in melting snowflakes is also documented in Fujiyoshi (1986). It is shown in Appendix B that $\rho_{HV}(0)$ of monodispersed scatterers with random protuberances is given in the Rayleigh limit as

$$|\rho_{HV}(0)| = (1 + 3\sigma_D^2/D^2)^2/(1 + 15\sigma_D^2/D^2 + 45\sigma_D^4/D^4 + 15\sigma_D^6/D^6), \quad (11)$$

where σ_D is the rms value of the protuberance and D is the equivalent diameter of the scatterer. Plot of Eq. (11) indicates (Fig. 7) that σ_D/D of 0.1 may reduce the correlation to 0.92. We expect similar or larger effects to be produced by Mie scatterers with protuberances; this we deduce from the fact that large, oblate, randomly oriented hail decreases the correlation (Fig. 6a).

When precipitation medium is rain, the shape effect is possibly the dominant cause for the changes in $\rho_{HV}(0)$. However, when the precipitation habitats include hailstones or snowflakes, the changes in $\rho_{HV}(0)$ are due to the cumulative effects of all the physical factors described so far.

f. *Mixture of two types of hydrometeors*

Precipitation below the melting level consists of a varying mixture of hydrometeors of diverse shape, size,

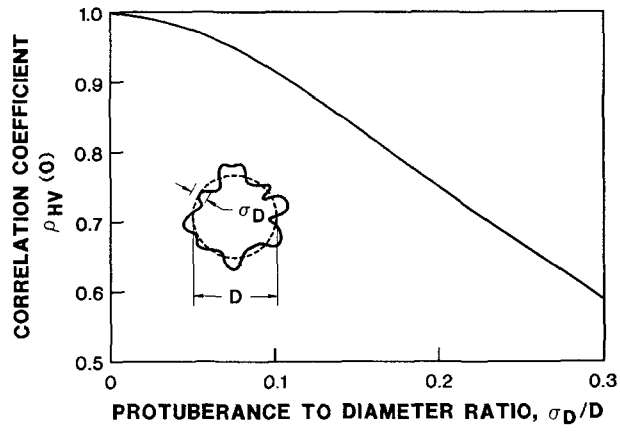

FIG. 7. Correlation coefficient for Rayleigh scatterers with protuberances.

and thermodynamic phase. It is common to observed mixed-phase precipitation that comprises either rain and hail near and below the melting level or graupel and hail mixtures above (Pruppacher and Klett 1978). In snow storms, mixtures of dry and wet snow of different shapes and sizes are found. The presence of such mixtures results in an observable decrease in $\rho_{HV}(0)$. This effect makes it possible to rapidly identify the bright band from the measurements of $\rho_{HV}(0)$ (Illingworth and Caylor 1989). Here we consider the effect of the mixture of rain and hail on $\rho_{HV}(0)$. Hailstones collected at the ground indicate that the hail size distribution is well represented by exponential functions (Matson and Huggins 1980; Cheng and English 1983). The observations of Carte and Held (1978) reveal that sometimes showers of large hail are nearly monodispersed. Ziegler et al. (1983) found that a gamma distribution is better suited. We consider two hailstone distributions. The first one is the exponential type given by Cheng and English (1983). The second is uniform size distribution centered around a mean hail size. The width of the distribution is taken to be 1 cm. The latter model is a closer approximation to the gamma and the nearly monodispersed size distributions. It allows us to isolate the effects of hail size on the polarimetric measurables. The rain drops are assumed to follow the Marshall-Palmer distribution. The hailstones are assumed to have a fixed axis ratio (0.5, 0.6, 0.7, 0.8 or 0.9). All hailstones are modeled as oblate spheroids oriented with their minor axes uniformly distributed in the horizontal plane [Eq. (10)]; that is because there is no preferential orientation with respect to the radar in the horizontal plane.

Figures 8a (wet hail) and 8b (spongy hail) show variation of ρ_{HV} in a mixture of rain and hail when the hailstone size distribution is taken as that given by Cheng and English (1983). A constant rain rate of 75 mm h^{-1} is assumed, in order to be compatible with the radar observations of mixed phase precipitation presented in section 5. The rain rate is obtained from the measurements of K_{DP}, which are not affected by hail (Balakrishnan and Zrnić 1990). Graphs on the figures stop at a reflectivity factor of 70 dBZ. Note that the correlation decreases with increasing hail rate (and thus size) and with decreasing axis ratio. Also the decrease with hail rate is not monotonic, but exhibits a minimum. The minimum value of $\rho_{HV}(0)$ is not strongly dependent on the amount of rain in the mixture, but the hail rate at $\rho_{HV}(0)$ minimum is. The minimum in Fig. 8 can be explained by the increasing contribution to the correlation coefficient from hail stones. It occurs at a point where rain and hail contributions to echo power are comparable because then the difference in the dependence of Z_H on size from the dependence of Z_V on size is largest. Beyond the minimum, hailstones dominate and ρ_{HV} increases. The dominance of the hailstones in the mixture is also indicated by the flat part of Z_{DR} curves shown in Figs. 9a and 9b for

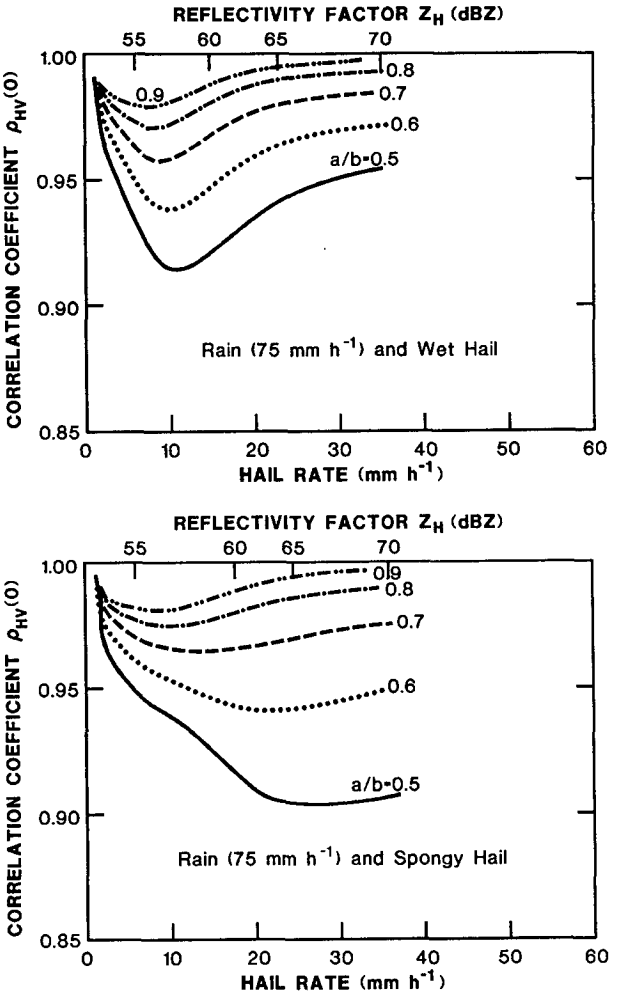

FIG. 8. Correlation coefficient for (a) a mixture of rain (75 mm h^{-1}) and wet hail. Cheng and English (1983) size distribution is used for hail. Axis ratios are indicated. The minor axis of oblate hailstones is randomly oriented in the horizontal plane. (b) As in (a) but for a mixture of rain (75 mm h^{-1}) and spongy hail.

the same model. Thus it is obvious from Figs. 8 and 9 that ρ_{HV} minimum is for mixed hydrometeors between pure rain and pure hail.

Size effect in dry hail becomes noticeable only when hailstones larger than about 5.5 cm are present. The effect is much more significant with wet and spongy hail, and it first occurs at a size of about 2 cm. At a size of about 4.5 cm both spongy and wet hail can produce a measurable change in $\rho_{HV}(0)$.

In actual precipitation, rapidly melting hailstones do not exhibit shapes with constant axis ratio (Rasmussen et al. 1984) and hence $\rho_{HV}(0)$ will be lower than that shown in Fig. 8. This is also seen in our measurements presented in section 5.

The dependence of the correlation coefficient on hailstone size is illustrated in Fig. 10a, where uniform distribution of hailstone size over a 1 cm size interval

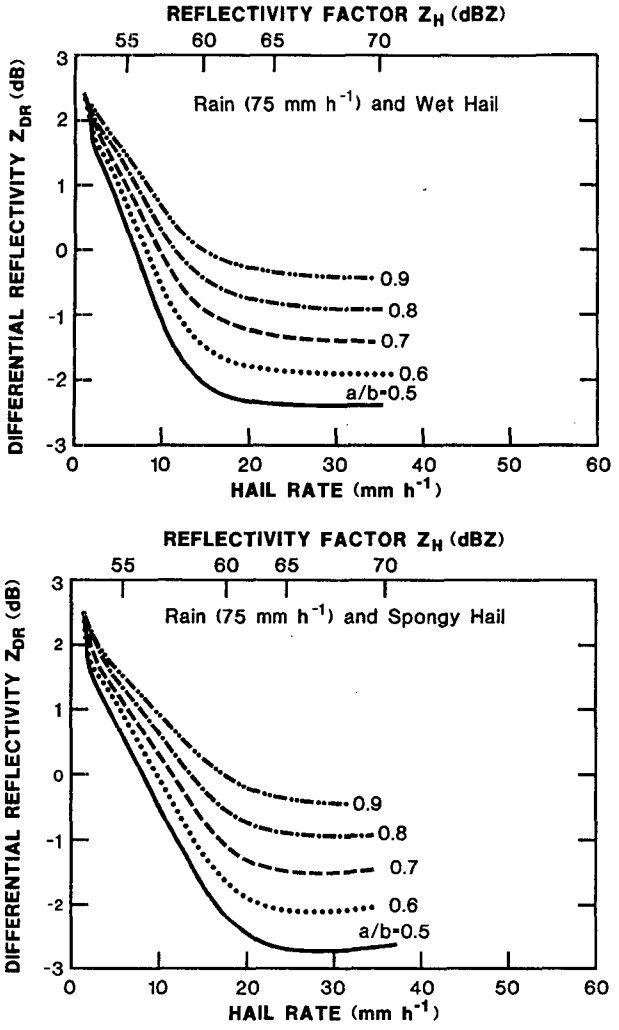

FIG. 9. As in Fig. 8 but for differential reflectivity.

is assumed. The rain rate is chosen to be 75 mm h^{-1}, and the hail rate is selected so that the total Z_H of the mixture is 65 dBZ, because these values were measured in our data. Figure 10a clearly demonstrates that the Mie scattering effects produce a decrease in ρ_{HV} near 1.5 and 5 cm and the decorrelation effects are larger for echoes from spongy hail. The variation of Z_{DR} for the same model is given in Fig. 10b. Figures 10a and 10b suggest that it might be possible to use Z_{DR} observations to overcome the ambiguity in ρ_{HV} and possibly categorize hail size if the postulated orientation occurs for sizes that are larger than a certain minimum size. Aerodynamic considerations and measurements suggest that this indeed may be the case.

4. Possible applications of $\rho_{HV}(0)$

Theoretical and experimental evidence presented in section 3 points toward several possible uses of the correlation coefficient. In pure rain the values that we measured are larger than 0.97 and the theory predicts similar values from hydrometeors of one type (pure rain or snow) that have little variations in their canting angles. In mixtures of hydrometeors $\rho_{HV}(0)$ is lower. Illingworth and Caylor (1989) observed a value of 0.6 in the bright band 9 km away from their high-resolution (beamwidth = 0.25°) radar. We have not seen similar results, probably because our observations were not closer than 45 km and antenna beamwidth is 0.9°. Smoothing by the beam may have reduced such features if they were present in our data.

A correlation coefficient lower than about 0.97 indicates that hydrometeor population may consist of two different types or that the hydrometeors have very irregular shape and/or are wobbling. If two different types of hydrometeors are present the correlation coefficient has a minimum when the contribution to the echo power by one type is close to the contribution by the other type.

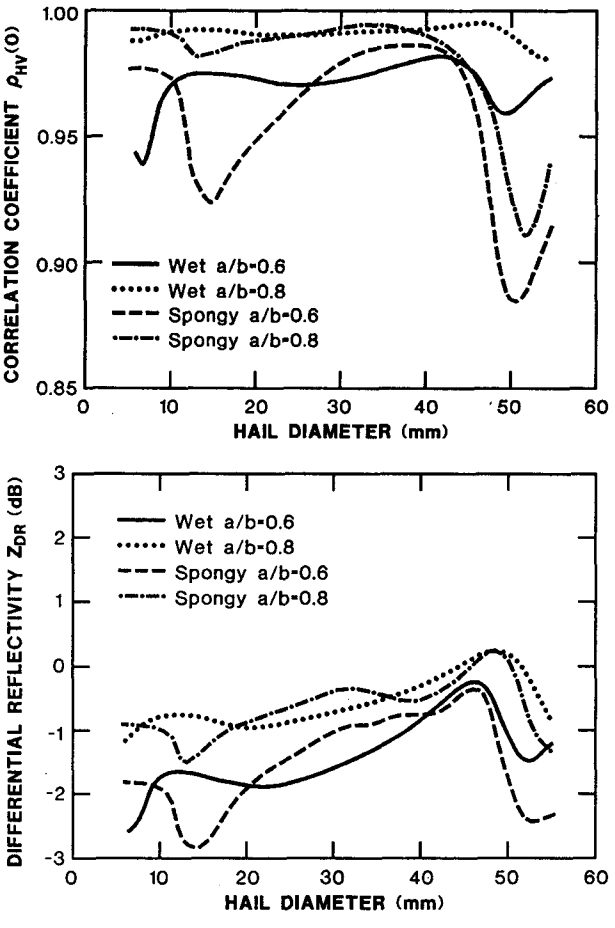

FIG. 10. (a) Correlation coefficient for a mixture of rain (75 mm h^{-1}) and hail; uniform hail distribution over 1-cm interval is assumed and the reflectivity factor is set to 65 dBZ. The x-axis denotes the center point of the sliding window distribution. The minor axis is oriented randomly in the horizontal plane. (b) Differential reflectivity of rain and hail mixture for the models represented in Fig. (a).

From the discussion in section 3 it follows that $\rho_{HV}(0)$ may have a potential to characterize hail size. Four independent factors cause a decrease in correlation. First, recall a sharp drop due to Mie scattering for hail sizes larger than 5 cm if shapes are oblate and hail is wet or spongy. Second, large hail (>4 cm) is often roughly spherical or irregular with small ar large protuberances (List 1985) that reduce the correlation. Third, in a mixture of hail and rain the correlation decreases with the size of the hailstones. Fourth, if hail size distribution is wide there would be both large and small hailstones; therefore the shape variety would be more pronounced and that would tend to decrease the correlation. Admittedly the listed causes are qualitative, but with other supporting information it may be possible to infer a few categories of sizes. The differential reflectivity may just be the other variable that could help in the hail estimation process.

The small amount of experimental information available about the shape of hail stones suggests that roughly oblate forms constitute about 75% (Barge and Isaac 1973) and that the oblateness weakly increases with size (Knight 1986). If this is correct and if the stones fall with minor axis horizontal (Knight and Knight 1970) then larger hail would produce larger negative Z_{DR}. We have examined a model wherein the minor axis is randomly oriented in the horizontal plane and have obtained differential reflectivity values between −0.5 and −2 dB. Larger magnitudes correspond to wet or spongy hail with larger oblateness (Fig. 10b). Negative Z_{DR} has been observed by Illingworth et al. (1987) as well as by Bringi et al. (1986), and by Husson and Pointin (1989); the negative Z_{DR} occurred in regions of maximum reflectivity and may have been produced by hail similar to that in our model. Bringi et al. (1986) also examined a model of oblate hail different from ours only in that it including canting and had a fixed azimuthal orientation so that the principal elliptic cross section was in the plane of polarization. The model reproduced essential features of their measurements. Although this is encouraging we caution the reader that models developed so far (including ours) can only provide plausible arguments because it is not known how hailstones fall and their shape may not be close to spheroidal.

5. Radar measurement and interpretation

We turn now to two observations of hail with a polarimetric radar in Oklahoma. Data from two storms that produced rain mixed with hail over Oklahoma on 2 June 1985, and 14 May 1986, are presented in Figs. 11a and 11b. A fairly detailed description and analysis of these two cases is given by Balakrishnan and Zrnić (1990) except that $\rho_{HV}(0)$ was not considered. The vertical profiles of Z, Z_{DR}, K_{DP}, and $\rho_{HV}(0)$ measured during the two storms show some similarities and also significant differences. Walnut-size hail was observed on the ground on 2 June (Fig. 11a) but hail smaller than 1 cm fell on 14 May (Fig. 11b). Reflectivity factors for both cases are similar and are typical of convective hailstorms. On the basis of this, one would expect little difference in type and size. Differences in other measurables, particularly $\rho_{HV}(0)$, and deeper subzero region, point out that hail was larger in the 2 June case. Negative Z_{DR} extends to 10 km, suggesting according to our model (Figs. 9a and 9b) larger vertically aligned hailstones; K_{DP} increases from the top of the melting layer to the ground, indicating that the dominant effect may be melting (Balakrishnan and Zrnić 1990) as opposed to breakup and coalescence, which might explain the decrease in K_{DP} below 1.5 km in Fig. 11b.

Above the melting layer, Z_{DR} (0 dB) and K_{DP} 0° km^{-1}) for the 14 May case could mean that the hydrometeors are either tumbling or of spherical shape; this is also consistent with $\rho_{HV}(0)$ which is nearly unity (see Fig. 6a for dry hail). However for the 2 June case, Z_{DR} and $\rho_{HV}(0)$ exhibit variations that are similar to a model of dry oblate hailstones oriented with minor axis horizontal as described in Section 3d(2). We speculate that some graupel may also be present above 6 km in the region where the correlation dips to 0.98. The increase of Z_{DR} to 0 at 4.8 km (the height of the 0 C°) is caused by the onset of melting; note that $\rho_{HV}(0)$ begins to decrease.

Below the melting level Z_{DR} grows monotonically in the 14 May case, indicating an ongoing melting process. However the negative Z_{DR} for the 2 June case suggests that raindrops and other horizontally elongated hydrometeors contributed little to it. It appears that as hailstones became wetter and possibly spongy on the way to the ground, Z_{DR} grew more negative. Oblate hailstones with an axis ratio of about 0.8 produce a Z_{DR} of −0.5 dB when they are dry and −1 dB when they are spongy or wet (Fig. 6b). Even larger values are obtained from more oblate hailstones ($a/b = 0.6$). But part of the decrease in Z_{DR} could be caused by intervening rain that creates differential attenuation. We have quantified differential attenuation using reflectivity data along the radial and assuming a Marshall–Palmer drop size distribution. (Note that polarimetric data could not be used for that purpose because they start at a range of 82.5 km whereas the reflectivity is available at all ranges.) The real part of the differential propagation constant for a given rain rate is obtained from scattering coefficients (for horizontal and vertical polarization) of rain drops comprising the distribution. The cumulative value of differential attenuation between the radar and the location (84 km) where Z_{DR} was measured turned out to be less than 0.4 dB at elevations below the melting level. Above the melting level differential attenuation is negligible. Another contributor to the negative Z_{DR} below the melting level may be by streamers of water detaching from the top side of hailstones. But this can not explain the negative values above the freezing level. One more factor that

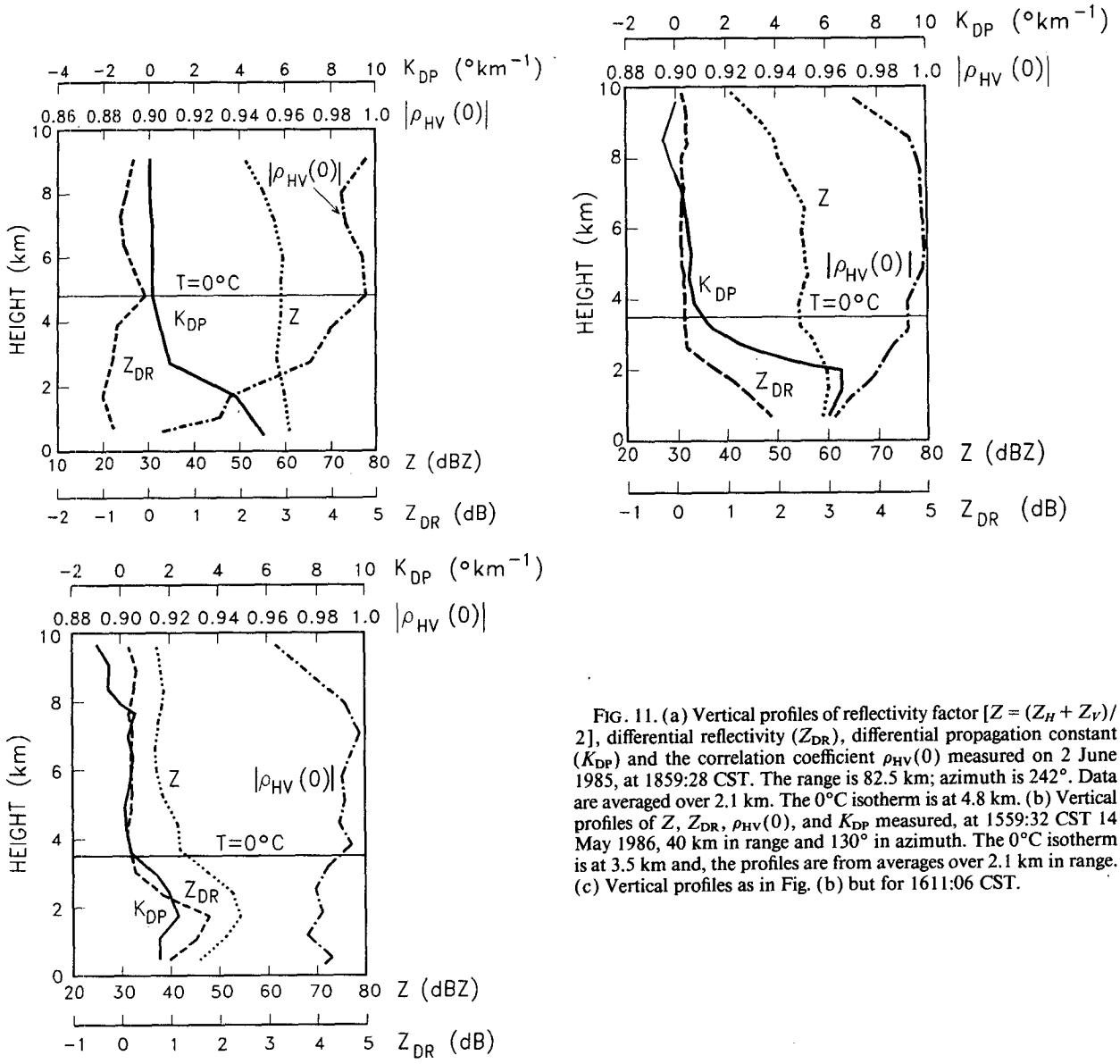

FIG. 11. (a) Vertical profiles of reflectivity factor [$Z = (Z_H + Z_V)/2$], differential reflectivity (Z_{DR}), differential propagation constant (K_{DP}) and the correlation coefficient $\rho_{HV}(0)$ measured on 2 June 1985, at 1859:28 CST. The range is 82.5 km; azimuth is 242°. Data are averaged over 2.1 km. The 0°C isotherm is at 4.8 km. (b) Vertical profiles of Z, Z_{DR}, $\rho_{HV}(0)$, and K_{DP} measured, at 1559:32 CST 14 May 1986, 40 km in range and 130° in azimuth. The 0°C isotherm is at 3.5 km and, the profiles are from averages over 2.1 km in range. (c) Vertical profiles as in Fig. (b) but for 1611:06 CST.

must be considered is the contamination through antenna sidelobes. Because the one way sidelobes are more than 20 dB below the main lobe, which in this case is illuminating maximum reflectivity core to a height of 8 km, this contamination is insignificant. Thus, the vertical profile of Z_{DR} could have been produced by a distribution of approximately oblate hailstones oriented with the minor axis horizontal.

Most striking is the systematic decrease of $\rho_{HV}(0)$. Because the decrease can be seen below the melting level in both cases, we deduce that the presence of mixed-phase hydrometeors was mainly responsible for it (see Figs. 8a, 8b and 10a as well as related discussion). Influence of protuberances if any is not significant because they would have produced Z_{DR} close to 0 dB. As expected, with larger hail sizes the decrease is significantly bigger in the 2 June case. Our model of mixed hail and rain predicts a smaller decrease (Fig. 8), most likely because it does not account for all the effects. Nevertheless the agreement is good, daring us to speculate about the hail size. Considering that the axis ratios smaller then 0.8 seems to fit our 2 June data better we turn to the results of Knight (1986) which show that hailstones larger than 2 cm have such axis ratios. Also, Husson and Pointin (1989) had negative Z_{DR} similar to ours and have measured, with hail pads, maximum sizes of 2.3 cm. Actual sizes aloft were most likely larger because of melting and because hail pads underestimate the maxima by about 50% (Smith and Waldvogel 1989). There are also reports from observers (*Storm Data* 1986) that refer to walnut size hail on 2 June. The evidence, indirect as it may be, implies that the

sizes were larger than 2 cm but smaller than 5 cm. Had there been hailstones larger than 5 cm a significantly larger drop in $\rho_{HV}(0)$ would have occurred and Z_{DR} would have a distribution around zero, neither of which is shown in our data. On the other hand, model calculations (Balakrishnan and Zrnić 1990) and radar data (Fig. 11b and other not shown) imply, and observations on the ground confirm that small hail (<1 cm) on 14 May was almost spherical or slightly oblate and was imbedded in heavy rain (100 mm h^{-1}). Calculated correlation of 0.972 for such a model is very close to the observed 0.96, considering that theory does not include other decorrelating effects such as oscillation, noise, and non-Gaussian spectral shapes; statistical bias alone causes a drop of about 0.007 in the estimate of $\rho_{HV}(0)$.

The vertical profiles in Fig. 11c correspond to the time when rain was observed on the ground on 14 May 1986. Here Z, Z_{DR}, and K_{DP} show that the precipitation has changed to stratiform type. As expected, $\rho_{HV}(0)$ at ground level increases to nearly unity—typical of its value in rain. It changes only in the region below the melting level where heterogeneous hydrometeors such as snow aggregates, water drops and/or the melting hailstones may coexist.

6. Conclusions

From the very first observation of precipitation by weather radars the scientific community has attempted to quantitatively discriminate between hydrometeors. As a matter of fact that was the primary activity of radar meteorologists until the advent of Doppler systems. During the last two decades multiparameter measurements of precipitation have been vigorously investigated and some remarkable strides have been made with polarimetric radars. Although there are other multiparameter techniques such as dual wavelength and radar–radiometer combination, the polarimetric concept allows a single instrument to be used and is thus a likely practical candidate for operational applications. The basic problem facing polarimetric researchers consists of deciding what variables to measure and how to relate them to the hydrometeors. We were spared the first decision by the fact that the existing radar measures dual linear (horizontally, vertically) polarized echoes in the main channel. Note that the orthogonal signals are also received but not processed, because of lack of a receiver for that purpose. Relating hydrometeors to polarimetric signatures especially in a quantitative sense is difficult. Put in simple terms a multiparameter decision rule is sought that will partition the four-dimensional space of Z_H, Z_{DR}, K_{DP} and $\rho_{HV}(0)$ so that each partition corresponds to a distinct hydrometeor population. We have made a small step in that direction with the following main results.

Pure rain produces a correlation coefficient between horizontally and vertically polarized echoes of 0.98. This measured value is consistent with theoretical predictions. Similar results are observed in other precipitation that contains hydrometeors of one type. In layman's terms the correlation is a measure of shape variations or irregularities in the radar resolution volume. Therefore, it decreases when diverse particles are present. Even then the values that we observed from echoes with good signal-to-noise ratios were not lower than 0.9. This is in full agrement with model results that we have obtained for a variety of rain and hail scenarios. Lower numbers were measured from noisy data, suggesting that $\rho_{HV}(0)$ could also be used for data quality control.

Significant monotonic decrease of the correlation coefficient was observed to start below the melting level in two storms that produced hail on the ground. In the one with small hail (<1 cm) correlation dropped to 0.96 whereas in the one with large hail (>2.5 cm) it dropped to 0.9. Theory predicts such behavior if hail and rain are mixed; gradual decrease of $\rho_{HV}(0)$ toward ground is caused by progressively increasing rain resulting from melting of hail. Different polarimetric measurables corroborate one another in suggesting that rain was mixed with hail. As a matter of fact a very good estimate of the rain in the mixture is made possible by the differential propagation constant measurements. On the basis of the model and these observations we believe that hail can be categorized into large and small with the inclusion of differential reflectivity into the consideration.

We have observed that differential reflectivity in the storm with large hail was negative throughout the core. Above the melting level the values were about −0.5 dB and below about −1 dB. Hailstones modeled as oblate spheroids with their minor axis randomly oriented in the horizontal plane and axis ratios between 0.6 and 0.8 reproduce all essential features of our measurements. Other investigators have noticed negative Z_{DR} in storms with large hail. Therefore it is tempting to attribute such observations to similar circumstances.

In summary, if hail larger than about 2 cm is mixed with rain it can be characterized by differential reflectivity values lower than about −0.5 dB and correlation coefficient lower than 0.94. We expect a similar threshold on differential reflectivity but no drop in the correlation for cases of wet or spongy hail without rain. Negative differential reflectivity between 0 and −0.5 dB from dry hail may also signify larger size although in our observation the presence of graupel could have been a factor. Although the current paper is based on limited observations, the strength of the study lies in the development of plausible models to explain the observations. Clearly many more observations are needed to generate enough statistical base to validate the models proposed herein.

Acknowledgments. The data used in this paper were a result a laboratory commitment and effort to which

many individuals contributed. D. Sirmans, J. Carter and M. Schmidt were instrumental in refurbishing the radar, and M. Schmidt also collected the data. D. Forsyth and his staff facilitated the analysis by relentless efforts in the modernization of NSSL computing facilities. Perceptive discussions with R. J. Doviak and P. Mahapatra and their continued interest in this work are greatly appreciated. Yosepha Gal-Chen provided assistance in some aspects of data handling. The computer codes for the extended T-matrix method were given to us by V. N. Bringi and J. Vivekanandan. We benefitted by discussing with them and V. Chandrasekar and G. Lessins several aspects of this and related problems. Ms. Carole Holder helped with many aspects of manuscript preparation and editing and Ms. Joan Kimpel prepared the graphics. Part of this work was supported by the Joint Systems Program Office for the Next Generation Weather Radar.

APPENDIX A

Characteristics of $\rho_{HV}(0)$

1. Estimation of $\rho_{HV}(0)$

When transmission consists of alternating sequence of H and V polarizations, two assumptions are needed to estimate $\rho_{HV}(0)$. First, some a priori model for the power spectral shape such as Gaussian (Doviak and Zrnić 1984) is needed. Second, the correlation at lag $(2m + 1)T_s$ (where T_s is the pulse repetition time) is assumed to contain independent contributions from Doppler spectral broadening and $\rho_{HV}(0)$, so that it can be expressed as a product $\rho(2m + 1)\rho_{HV}(0)$, (Sachidananda and Zrnić 1986). The correlation due to Doppler spread at lag $2T_s$ is

$$\hat{\rho}(2) = \frac{\sum (H_{2i}H^*_{2i+2} + V_{2i+1}V^*_{2i+3})}{(M + 1)(\hat{P}_H + \hat{P}_V)}, \quad \text{(A1)}$$

where P_H and P_V are the mean sample powers at H and V polarizations, and M is the number of H and V sample pairs. An estimate of $\rho_{HV}(1)$ is obtained as

$$|\hat{\rho}_{HV}(1)| = \frac{|\hat{R}_a| + |\hat{R}_b|}{2(\hat{P}_H\hat{P}_V)^{0.5}}, \quad \text{(A2)}$$

where R_a is the autocorrelation between successive H and V polarized echoes and R_b is that between V and H polarized echoes.

The correlation coefficient is computed directly from Eqs. (A1) and (A2) as

$$\hat{\rho}_{HV}(0) = |\hat{\rho}_{HV}(1)/\hat{\rho}(1)|, \quad \text{(A3)}$$

since the assumption of Gaussian spectral shape permits equating $\rho(1)$ to $|\rho(2)|^{0.25}$.

2. Standard error in the estimate of $\rho_{HV}(0)$

The variance of $\rho_{HV}(0)$ is written using a perturbation expansion (Hahn and Shapiro 1967) as

$$\frac{\text{var}|\rho_{HV}(0)|}{|\rho_{HV}(0)|^2} = \frac{\text{var}|\rho_{HV}(1)|}{|\rho_{HV}(1)|^2} + (0.25)^2\frac{\text{var}|\rho(2)|}{|\rho(2)|^2} - \frac{(0.5)\,\text{cov}(|\rho(2)|, |\rho_{HV}(1)|)}{|\rho(2)| \cdot |\rho_{HV}(1)|} \quad \text{(A4)}$$

where all the correlations are estimates. The variances and the covariance in Eq. (A4) are obtained from one more perturbation analysis, this time of each estimate (Zrnić 1977). The normalized standard error of $\rho_{HV}(0)$ is plotted in Fig. A1 as a function of the number of sample pairs M and for the operational unambiguous velocity of 34 m s^{-1}. Values for other ratios of spectrum width to unambiguous velocity can be obtained directly from the graph.

We find that the normalized standard error in $\rho_{HV}(0)$ is better than 0.029 when the spectrum width is 1 m s^{-1} and M is 128. Range averaging over nine samples reduces this error to $\leq$0.01, which is sufficient for sensing the mixed-phase precipitation and gauging the hail size quantitatively. In rain medium (Fig. 2), the use of $\rho_{HV}(0)$ is likely to be limited by the standard error in its estimate, and hence only a qualitative assessment of the bias in Z_{DR} seems possible.

3. Bias in the estimate of $\rho_{HV}(0)$

The bias in the estimate can be calculated from a similar perturbation expansion as the one for the variance. It is given by the difference between the true and the estimated values as

$$\text{bias} = \frac{1}{2}\left[\frac{\text{var}|\rho_{HV}(0)|}{|\rho_{HV}(0)|^2} + 0.0625\frac{\text{var}|\rho(2)|}{|\rho(2)|^2} - 0.25|\rho(2)|^{-1.25}\,\text{cov}(|\rho_{HV}(0)|, |\rho(2)|)\right]. \quad \text{(A5)}$$

In Fig. A2 this bias is plotted as a function of the number of sample pairs M for representative spectrum widths and for an unambiguous velocity of 34 m s^{-1}. Note that the estimate is always smaller than the true value.

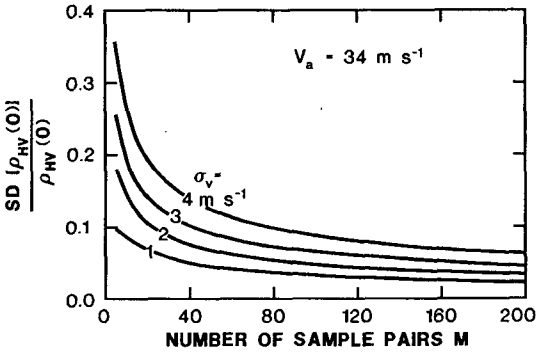

FIG. A1. Standard deviations in radar measurements of $\rho_{HV}(0)$. Unambiguous velocity is 34 m s^{-1} and spectrum width is indicated.

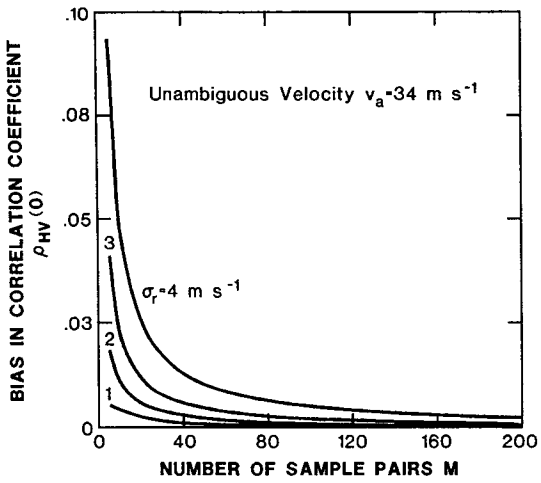

FIG. A2. Bias in $\rho_{HV}(0)$ for the same parameters as in Fig. A1.

APPENDIX B

Correlation $\rho_{HV}(0)$ for a distorted sphere

Derivation of Eq. (11) is given in this appendix. The backscattering coefficients for a spherical body distorted by protuberances can not be easily obtained unless some simplifying assumptions are made. Because the following calculations serve to illustrate general trends in the correlation coefficient as a function of distortions in sphericity and not to detail scattering effects of protuberances we consider only the Rayleigh approximation. This simplifies greatly the calculations but is not strictly correct for large hailstones even at a 10-cm wavelength. In this approximation the scattering coefficient S_H is

$$S_H = \pi^3 K_w D^3 / 2\lambda^2 \qquad \text{(B1)}$$

where K_w is related to the refractive index of water. An identical expression is obtained for the coefficient S_V. The phase shift due to scattering is neglected here because in the Rayleigh approximation it is the same for both horizontal and vertical polarizations. Therefore, there is no net phase shift in Eq. (1).

For distortions that are small compared to the diameter of the sphere we can assume that the scattering coefficient is proportional to $(D + \Delta_H)^3$ where $D + \Delta_H$ is the maximum dimension in the direction (horizontal in this case) of the incident electric field. That is to say, the dominant component of the backscattered field is horizontal and it is mainly affected by the length of the scatterer in the horizontal direction. The constant of proportionality need not be known as long as it is a constant or at least has a very weak dependence on the shape of the distortion. This is because in calculating the correlation coefficient [Eq. (1)] the constants in the numerator and denominator will cancel out.

One more assumption is needed in order to obtain a closed form solution for the correlation coefficient and that is that a protuberance in the vertical direction is independent of one in the horizontal direction. Although not strictly true this assumption is a good approximation for an ensemble of scatterers that have random protuberances and are randomly oriented.

Now we are in a position to calculate the expected value of the product $\langle S_H S_V^* \rangle$ as

$$\langle S_H S_V^* \rangle = C^2 \int N(D') I_H I_V^* dD' \qquad \text{(B2)}$$

where C is a constant incorporating the values independent of the diameter D and the perturbations. The I_H and I_V are integrals involving an assumed distribution of protuberance amplitudes $p(\Delta_H)$. We list here only I_H because I_V can be obtained by simply replacing subscripts H with V. Thus

$$I_H = \int (D' + \Delta_H)^3 p(\Delta_H) d\Delta_H. \qquad \text{(B3)}$$

For a symmetric distribution of Δ_H (and Δ_V) the integral (B3) becomes

$$I_H = (D^3 + 3D\sigma_D^2) \qquad \text{(B4)}$$

where σ_D is the rms value of Δ_H. I_V is identical to I_H so that (B2) can be evaluated readily. We consider a monodispersed distribution of scatterers [i.e., $N(D') = \delta(D' - D)$] so that the expectation (B2) reduces to

$$\langle S_H S_V^* \rangle = C^2 (D^3 + 3D\sigma_D^2)^2. \qquad \text{(B5)}$$

One more computation is needed, namely the value of $\langle |S_H|^2 \rangle$ or $\langle |S_V|^2 \rangle$. These are equal and can be evaluated in closed form if the probability density function $p(\Delta_H)$ is known. We take a Gaussian density which allows higher order moments of Δ_H to be expressed in terms of the second order moment σ_D^2. Following the procedure for computing (B3) we obtain

$$\langle |S_H|^2 \rangle = C^2 (D^6 + 15D^4\sigma_D^2 + 45D^2\sigma_D^4 + 15\sigma_D^6). \qquad \text{(B6)}$$

Finally the ratio of Eq. (B5) to Eq. (B6) produces Eq. (11) of the paper.

REFERENCES

Antar, A. M. M., and A. A. Hendry, 1985: Correlation measurements in precipitation at linear polarization using dual-channel radar. *Electron. Lett.*, **21**, 1052–1054.

Aydin, K., T. A. Seliga and V. Balaji, 1986: Remote sensing of hail with a dual linear polarization radar. *J. Climate Appl. Meteor.*, **25**, 1475–1484.

Balakrishnan, N., and D. S. Zrnić, 1989: Suggested use of the cross-correlation between orthogonally polarized echoes to infer hail size. *Preprints, 24th Conference on Radar Meteorology*, Tallahassee, Amer. Meteor. Soc., 292–296.

——, and ——, 1990: Estimation of rain and hail rates in mixed phase precipitation. *J. Atmos. Sci.*, **47**, 565–583.

Barber, P., and C. Yeh, 1975: Scattering of electromagnetic waves by arbitrarily shaped dielectric bodies. *Appl. Opt.*, **14**, 2864–2872.

Barge, L. G., 1972: Hail detection with a polarization diversity radar. Stormy Weather Group Scientific Report, MW-71, McGill University, Canada.

Barge, B. L., and G. A. Isaac, 1973: The shape of Alberta hailstones. *J. Rech. Atmos.*, **7**, 11–20.

Battan, L. J., 1966: *Radar Meteorology,* University of Chicago Press.

Born, M., and E. Wolf, 1964: *Principles of Optics,* 2nd ed., Macmillan.

Bringi, V. N., R. M. Rasmussen and J. Vivekanandan, 1986a: Multiparameter radar measurements in Colorado convective storms. Part I: Graupel melting studies. *J. Atmos. Sci.*, **43**, 2545–2563.

——, J. Vivekanandan and J. D. Tuttle, 1986b: Multiparameter radar measurements in Colorado convective storms, Part II: Hail detection studies. *J. Atmos. Sci.*, **43**, 2564–2577.

Carte, A. E., and G. Held, 1978: Variability of hailstorms on the South African plateau. *J. Appl. Meteor.*, **17**, 365–373.

Cheng, L., and M. English, 1983: A relationship between hailstone concentration and size. *J. Atmos. Sci.*, **40**, 204–213.

Doviak, R. J., and D. S. Zrnić, 1984: *Doppler Radar and Weather Observations,* Academic Press, 458 pp.

Fujiyoshi, Y., 1986: Melting snowflakes. *J. Atmos. Sci.*, **43**, 307–311.

Goddard, J. W. F., and S. M. Cherry, 1984: The ability of dual-polarization radar (copular linear) to predict rainfall rate and microwave attenuation. *Radio Sci.*, **19**, 201–208.

Green, A. W., 1975: An approximation for the shape of large raindrops. *J. Appl. Meteor.*, **14**, 1578–1583.

Hahn, J. H., and S. S. Shapiro, 1967: *Statistical Models in Engineering,* Wiley, 355 pp.

Hendry, A., G. C. McCormick and L. G. Barge, 1976: The degree of common orientation of hydrometeors observed by polarization diversity radar. *J. Appl. Meteor.*, **15**, 633–640.

Holt, A. R., 1984: Some factors affecting the remote sensing of rain by polarization diversity radar in the 3 to 35 GHz frequency range. *Radio Sci.*, **19**, 1399–1412.

Husson, D., and Y. Pointin, 1989: Quantitative estimation of the hail fall intensity with a dual polarization radar and a hailpad network. Preprints, *24th Conference on Radar Meteorology,* Tallahassee, Amer. Meteor. Soc., 318–321.

Illingworth, A. J., and I. J. Caylor, 1989: Cross polar observations of the bright band. *Preprints, 24th Conference on Radar Meteorology,* Tallahassee, Amer. Meteor. Soc., 323–327.

——, J. W. F. Goddard and S. M. Cherry, 1987: Polarization studies of precipitation development in convective storms. *Quart. J. Roy. Meteor. Soc.*, **113**, 469–489.

Jameson, A. R., 1983: Microphysical interpretation of multi-parameter radar measurements in rain. Part I: Interpretation of polarization measurements and estimation of raindrop shapes. *J. Atmos. Sci.*, **40**, 1792–1802.

——, 1985: Microphysical interpretation of multiparameter radar measurements in rain, Part III: Interpretation and measurements of propagation differential phase shift between orthogonal linear polarizations. *J. Atmos. Sci.*, **42**, 607–614.

——, 1987: Relations among linear and circular polarization parameters measured in canted hydrometeors. *J. Atmos. Oceanic Technol.*, **4**, 634–645.

——, and E. A. Mueller, 1985: Estimation of propagation-differential phase shift from sequential orthogonal linear polarization radar measurements. *J. Atmos. Oceanic Technol.*, **2**, 133–137.

——, and J. H. Dave, 1988: An interpretation of circular polarization measurements affected by propagation differential phase shift. *J. Atmos. Oceanic Technol.*, **5**, 405–415.

Knight, N. C., 1986: Hailstone shape factor and its relation to radar interpretation of hail. *J. Climate Appl. Meteor.*, **25**, 1956–1958.

Knight, C. A., and N. C. Knight, 1970: The falling behavior of hailstones. *J. Atmos. Sci.*, **27**, 672–681.

Kry, P. R., and R. List, 1974: Angular motions of freely falling spheroidal hailstone models. *Phys. Fluids,* **17**, 1093–1102.

Leitao, M. J., and P. A. Watson, 1984: Application of dual linearly polarized radar data to prediction of microwave path attenuation at 10–30 GHz. *Radio Sci.*, **19**, 209–221.

List, R., 1985: Properties and growth of hailstones. *Thunderstorm Dynamics and Morphology,* E. Kessler, Ed., University of Oklahoma Press, 259–276.

Longtin, D. R., C. F. Bohren and L. J. Battan, 1987: Radar backscattering by large, spongy ice oblate spheroids. *J. Atmos. Oceanic Technol.*, **4**, 355–358.

Matson, R. J., and A. W. Huggins, 1980: The direct measurement of the sizes, shapes and kinematics of falling hailstones. *J. Atmos. Sci.*, **37**, 1107–1125.

McCormick, G. C., 1979: Relationship of differential reflectivity to correlation in dual-polarization radar. *Electron. Lett.*, **15**, 265–266.

——, and A. Hendry, 1975: Principles for the radar determination of the polarization properties of precipitation. *Radio Sci.*, **10**, 421–434.

Meischner, P., T. Jank, V. N. Bringi and J. Vivekanandan, 1989: Multiple-plane ZDR measurements in convective and stratiform clouds using the C-band polarimetric DVFLR radar. Preprints, *24th Conference on Radar Meteorology,* Tallahassee, Amer. Meteor. Soc., 342–347.

Metcalf, J. I., 1988: A new slant on the distribution and measurement of hydrometeor canting angles. *J. Atmos. Oceanic Technol.*, **5**, 571–578.

Mueller, G. A., 1984: Calculation procedure for differential propagation phase shift. *Preprints, 22nd Conference on Radar Meteorology,* 10–13 September, Zurich, Amer. Meteor. Soc., 397–399.

National Climatic Data Center, 1985: *Storm Data,* Vol. 27, Asheville, NC.

——, 1986: *Storm Data,* Vol. 28, Asheville, NC.

Pruppacher, H. R., and R. L. Pitter, 1971: A semi-empirical determination of the shape of cloud and rain drops. *J. Atmos. Sci.*, **28**, 86–94.

——, and J. D. Klett, 1978: *Microphysics of Clouds and Precipitation,* Reidel.

Rasmussen, R. M., V. Levizzani and H. R. Pruppacher, 1984: A wind tunnel and theoretical study of the melting behavior of atmospheric ice particles, Part III: Experiment and theory for spherical ice particles of radius > 500 μm. *J. Atmos. Sci.*, **41**, 381–388.

Sachidananda, M., and D. S. Zrnić, 1985: Z_{DR} measurement considerations for a fast scan capability radar. *Radio Sci.*, **20**, 907–922.

——, and ——, 1986: Differential propagation phase shift and rainfall rate estimation. *Radio Sci.*, **21**, 235–247.

——, and ——, 1987: Rain rate estimates from differential polarization measurements. *J. Atmos. Oceanic Technol.*, **4**, 588–598.

Seliga, T. A., and V. N. Bringi, 1976: Potential use of radar differential reflectivity measurements at orthogonal polarizations for measuring precipitation. *J. Appl. Meteor.*, **15**, 69–76.

——, and ——, 1978: Differential reflectivity and differential phase shift: Applications in radar meteorology. *Radio Sci.*, **13**, 271–275.

Smith, P. L., and A. Waldvogel, 1989: On the determination of maximum hailstone sizes from hailpad observations. *J. Appl. Meteor.*, **28**, 71–76.

Stapor, D. T., and T. Pratt, 1984: A generalized analysis of dual-polarization measurements of rain. *Radio Sci.*, **19**, 90–98.

Ulbrich, C. W., and D. Atlas, 1984: Assessment of the contribution of differential polarization to improved rainfall measurements. *Radio Sci.*, **19**, 49–57.

Warner, C., 1978: Calculated scattering characteristics of hailstones at weather radar wavelengths. Contract Rep., Dept. Environ. Sci., University of Virginia.

Ziegler, C. L., P. S. Ray and N. C. Knight, 1983: Hail growth in an Oklahoma multicell storm. *J. Atmos. Sci.*, **40**, 1768–1791.

Zrnić, D. S., 1977: Spectral moment estimates from correlated puls pairs. *IEEE Trans. Aerosp. Electron. Syst.*, **AES-13**, 281–289.

——, N. Balakrishnan and M. Sachidananda, 1988: Processing and interpretation of alternately polarized weather radar echoes. *Proc., IGARSS,* No. ESA SP-284, 243–246.